Blocking Statistics in a Varying Climate: Lessons from a "Traffic Jam" Model with Pseudostochastic Forcing

ADIV PARADISE

Department of Astronomy, University of Toronto, Toronto, Ontario, Canada

CESAR B. ROCHA

Woods Hole Oceanographic Institution, Woods Hole, Massachusetts

PRAGALLVA BARPANDA AND NOBORU NAKAMURA

Department of the Geophysical Sciences, University of Chicago, Chicago, Illinois

(Manuscript received 14 April 2019, in final form 2 July 2019)

ABSTRACT

Recently Nakamura and Huang proposed a semiempirical, one-dimensional model of atmospheric blocking based on the observed budget of local wave activity in the boreal winter. The model dynamics is akin to that of traffic flow, wherein blocking manifests as traffic jams when the streamwise flux of local wave activity reaches capacity. Stationary waves modulate the jet stream's capacity to transmit transient waves and thereby localize block formation. Since the model is inexpensive to run numerically, it is suited for computing blocking statistics as a function of climate variables from large-ensemble, parameter sweep experiments. We explore sensitivity of blocking statistics to (i) stationary wave amplitude, (ii) background jet speed, and (iii) transient eddy forcing, using frequency, persistence, and prevalence as metrics. For each combination of parameters we perform 240 runs of 180-day simulations with aperiodic transient eddy forcing, each time randomizing the phase relations in forcing. The model climate shifts rapidly from a block-free state to a block-dominant state as the stationary wave amplitude is increased and/or the jet speed is decreased. When eddy forcing is increased, prevalence increases similarly but frequency decreases as blocks merge and become more persistent. It is argued that the present-day climate lies close to the boundary of the two states and hence its blocking statistics are sensitive to climate perturbations. The result underscores the low confidence in GCM-based assessment of the future trend of blocking under a changing climate, while it also provides a theoretical basis for evaluating model biases and understanding trends in reanalysis data.

1. Introduction

The general circulation of Earth's extratropical troposphere is dominated by traveling weather systems (ridges and troughs) embedded in the westerly winds of the jet stream. Occasionally the jet stream develops an anomalous, persistent meandering in a certain region and disrupts the normal eastward migration of these weather systems: a condition known as blocking. The stalled ridges and troughs cause heat waves, droughts, prolonged rain, and other abnormal weather patterns. Due to its association with climate extremes, blocking and its response to climate change have been studied extensively (e.g., Woollings et al. 2018, and references therein). Despite its impact on society, blocking remains a challenging problem in numerical weather prediction (Pelly and Hoskins 2003; Jia et al. 2014) and particularly in future climate projections (Woollings et al. 2018). In fact, a precise definition of a block itself is somewhat elusive because of its multifaceted characteristics. Many indices have been proposed, and while most produce consistent climatologies, they often disagree in identifying individual events and in evaluating

Denotes content that is immediately available upon publication as open access.

Supplemental information related to this paper is available at the Journals Online website: https://doi.org/10.1175/JAS-D-19-0095.s1.

Corresponding author: Noboru Nakamura, nnn@uchicago.edu

DOI: 10.1175/JAS-D-19-0095.1

the effects of climate change on the statistics of blocking (Barnes et al. 2012, 2014).

The difficulty stems partly from the lack of definitive theory for the onset of persistent jet anomalies. Proposed theories for block formation and maintenance include resonance between stationary Rossby waves and forcing (Charney and DeVore 1979; Tung and Lindzen 1979; Brunet 1994; Petoukhov et al. 2013), modon in a shear flow (McWilliams 1980; Malguzzi and Malanotte-Rizzoli 1984; Haines and Marshall 1987; Butchart et al. 1989), interaction between transient eddies and a diffluent flow (Shutts 1983; Colucci 1985, 2001; Trenberth 1986; Mullen 1987; Nakamura and Wallace 1993; Nakamura et al. 1997; Luo 2000, 2005; Altenhoff et al. 2008), instability/nonlinearity of low-frequency circulation (Swanson 2000; Cash and Lee 2000), selective absorption of vorticity anomalies (Yamazaki and Itoh 2009), and diabatic forcing from moist processes (Pfahl et al. 2015). Some of these theories are conceptual and difficult to verify with data directly, whereas others are more diagnostic and do not have predictive skill. Incomplete theoretical understanding hinders interpretation of blocking statistics and its response to climate perturbation in simulations and reanalysis products.

Recently Nakamura and Huang (2018, hereafter NH18) proposed a semiempirical theory for block formation based on the observed budget of local wave activity (LWA). LWA is the amplitude of Rossby wave measured by the meridional displacement of quasigeostrophic potential vorticity (PV) from zonal symmetry (Huang and Nakamura 2016, 2017). NH18 showed that major blocks that develop in the exit regions of the storm tracks in the Northern Hemisphere winter are associated, on average, with a converging along-stream flux of LWA, which is dominated by zonal advection (Figs. 4 and 5c of NH18). The convergence occurs when an increasing LWA decelerates westerly winds to the point that the advective LWA flux stops growing, which defines the "capacity" of the jet stream for the Rossby wave transmission. The dynamics captured by their observation and theory is akin to that of traffic flow on a highway. Just as traffic jams form when traffic capacity of the highway is exceeded, blocks manifest when/where the capacity of the jet stream is reached for the Rossby wave traffic. As will be explained more fully in the next section, stationary waves modulate the capacity to transmit transient waves by creating confluence and diffluence of the jet stream (analogous to the variation in the speed limit on a highway) and localize block formation.

NH18 conceptualize this mechanism with a simple 1D nonlinear partial differential equation (PDE) [their Eq. (4), also Eq. (1) in the next section]. The model takes the stationary wave activity, transient eddy forcing, and the background group velocity (jet speed plus intrinsic group velocity) as prescribed external parameters and predicts the evolution of LWA associated with transient waves. It is capable of reproducing the salient features of the average North Atlantic blocking in winter (cf. Figs. 5 and 6 of NH18). The threshold of block formation is expressed in terms of the parameters of the model [their Eq. (5), also Eq. (4) below]. NH18 hypothesize that climate change affects blocking statistics by modifying the threshold condition. While we do not know precisely how climate change will affect the threshold, the model allows for a controlled variation of "climate states" spanned by the aforementioned parameters. The economy of the model is suited for conducting large-ensemble experiments over a wide range of parameter space, which is the main goal of this study. It is hoped that the behavior of model's statistics with respect to the threshold will give us a clue as to how blocking might respond to hypothetical climate perturbations. Given the simplicity of the model, we do not expect the result to provide a quantitatively accurate prediction of future blocking trends, and the model parameters considered herein are likely not independent of each other under the real climate change. Instead, our intention is to provide a theoretical basis for understanding the blocking behaviors for a broad range of climate conditions. The next section reviews the 1D model introduced by NH18 and describes the experimental design. Section 3 discusses the results, followed by a summary and discussion in the concluding section.

2. The model

NH18 propose the following 1D nonlinear PDE as a prototype of blocking dynamics:

$$\frac{\partial}{\partial t}\hat{A}(x,t) = -\frac{\partial}{\partial x}\{[C(x) - \alpha\hat{A}]\hat{A}\} + \hat{S}(x,t) - \frac{\hat{A}}{\tau} + \kappa\frac{\partial^2\hat{A}}{\partial x^2}. \tag{1}$$

Equation (1) describes the amplitude evolution of transient Rossby waves along the jet stream, expressed in terms of barotropic LWA $\hat{A}(x, t)$. (The other variables are to be explained below.) The equation is derived from the more general 3D conservation of LWA [Huang and Nakamura 2016, Eqs. (20)–(22)]:

$$\frac{\partial}{\partial t}A = -\nabla\cdot\mathbf{F} + \dot{A} \tag{2}$$

at a particular latitude with the assumption that the atmosphere is barotropic. In Eq. (2) LWA density A ($\geq$0) measures the meridional displacement of PV from zonal

symmetry, **F** is the generalized (3D) Eliassen–Palm (E-P) flux density including the zonal advection of LWA by a hypothetical wave-free reference state flow U_{REF}, and $\dot{A}$ is the nonconservative sources–sinks of A. NH18 construct a column budget of LWA from Eq. (2) and evaluate it with reanalysis data in the exit regions of the jet stream, identifying dominant terms. They find that the convergence of the zonal advective flux dominates the tendency of LWA on synoptic time scales and thus lump together the other unimportant terms into forcing and damping of LWA. Furthermore, they partition $A(x, t)$ into stationary and transient wave components as $A(x, t) \equiv A_0(x) + \hat{A}(x, t)$, where the stationary wave component A_0 is defined as the minimum value of A at x. By subtracting the equation for $A_0(x)$ from that for A, they arrive at Eq. (1) (see the supplementary materials of NH18).

The nonlinear zonal flux of $\hat{A}$ on the rhs of Eq. (1), $F(x, t) \equiv [C(x) - \alpha\hat{A}]\hat{A}$, plays the key role for block formation in this model. It arises from the empirical relation between the advecting zonal wind and LWA:

$$u(x,t) = U_{\mathrm{REF}} - \alpha A(x,t), \tag{3}$$

where u is the zonal wind and U_{REF} is a constant zonal wind of the wave-free reference state. The constant parameter α measures the strength of wave-zonal flow interaction. Using reanalysis data NH18 determined $\alpha \approx 0.55$ in the exit regions of the storm tracks in the boreal winter.[1] The $C(x) \equiv U_{\mathrm{REF}} + c_g - 2\alpha A_0(x)$ is the background group velocity in the reference state, $U_{\mathrm{REF}} + c_g$, modulated by the stationary wave $A_0(x)$. Half of the modulation reflects the deceleration of the advecting zonal wind by the stationary wave, whereas the remaining half reflects direct interaction of transient waves with the stationary wave. Note that the modification of the meridional PV gradient by the waves is implicit in A [generally, large A is associated with a reduced meridional PV gradient; Eq. (18) of Huang and Nakamura 2016]. As a packet of eastward propagating Rossby waves encounters a diffluent region of the jet stream maintained by the stationary wave, where $C(x)$ is small, the packet slows down and accumulates $\hat{A}$. Initially the increasing $\hat{A}$ increases the LWA flux F. However it also decelerates the zonal wind through Eq. (3), which acts to diminish the advective flux of $\hat{A}$. If $\hat{A}$ continues to grow, $F(x, t) = [C(x) - \alpha\hat{A}]\hat{A}$ eventually stops growing and reaches the maximum value, $F_{\max} = C^2/4\alpha$, at $\hat{A} = \hat{A}_c = C(x)/2\alpha$. This condition is expressed as

$$\Gamma(x,t) \equiv \frac{F}{F_{\max}} = \frac{4\alpha F}{C^2(x)} = 1, \quad \hat{A} = \hat{A}_c(x) = \frac{C(x)}{2\alpha}, \tag{4}$$

where $\Gamma(x, t)$ defines the saturation level of the transient LWA flux F (NH18). As $\hat{A}$ grows past the critical value $\hat{A}_c$, F starts to decrease and causes a runaway accumulation of wave activity, provided that there is a continued supply of wave activity from upstream. This leads to a rapid increase in $\hat{A}$ and a rapid drop in F, which characterize block formation (Nakamura and Huang 2017; NH18). Thus Eq. (4) may be viewed as a threshold for blocking onset. It is clear that a small $C(x)$ requires only a small F and $\hat{A}$ to reach the threshold and is therefore conducive to block formation. The stationary wave creates preferred regions for blocking by minimizing $C(x)$ locally, which typically correspond to the diffluent regions of the jet stream.

The second term on the rhs of Eq. (1), $\hat{S}(x, t)$, is transient eddy forcing including low-altitude baroclinic source (cyclogenesis), meridional divergence of eddy momentum flux, and diabatic heating (Huang and Nakamura 2016; NH18). The third term represents linear damping of LWA due to frictional, radiative and mixing processes with the damping time scale of τ. The last diffusion term is related to the correlation between PV and the zonal wind along the meridional path of displacement (see appendix A). This term also keeps the numerical solution smooth.

Equation (1) is highly idealized and not meant for accurate prediction of blocks in real weather. The model provides no direct connection to temperature or precipitation anomalies. Since the Rossby waves in the model only propagate zonally or are absorbed by blocks without being refracted meridionally, some details of blocking life cycle are likely misrepresented. Still Eq. (1) encapsulates canonical dynamics that produce persistent anomalies in the jet stream inferred from data, and it reproduces the salient features of blocking in the boreal winter when the threshold is reached (NH18). Nakamura and Huang (2017) also show that realistic wave breaking and blocking occur in a 2D model once the same threshold is reached, and that the zonal structure of the wave envelope is qualitatively similar to the 1D result (their Figs. 3 and 10).

Yet the true utility of Eq. (1) lies in its economy: it is suited for large ensemble runs in parameter sweep experiments and long-term calculations. We expect that the blocking threshold will shift when the parameters of the model are varied and affect the statistics of blocks.

[1] In the WKB limit of a plane wave in barotropic flow where Kelvin's circulation is conserved over one wavelength of the PV contour, Eq. (3) reduces to the local nonacceleration relation with $\alpha = 1$ (Huang and Nakamura 2016; Nakamura and Huang 2017).

TABLE 1. List of parameters.

Abbreviation and value/range	Description
Fixed parameters	
$L_x = 2.8 \times 10^7$ m	Length of the channel
$\alpha = 0.55$	Strength of wave–flow interaction
$\tau = 10$ days	Damping time scale of wave activity
$\kappa = 3.26 \times 10^5\ \mathrm{m^2\,s^{-1}}$	Diffusion coefficient for transient wave activity
$S_0 = 1.852 \times 10^{-5}\ \mathrm{m\,s^{-2}}$	Background eddy forcing
$N = 26$	Number of component waves in transient eddy forcing
$M = 21$	Number of component waves in stationary wave noise
Varied parameters	
$\gamma \in [0.5, 4]$ (default = 2)	Nondimensional strength of transient eddy forcing
$k_n \in [1, 20]$	Integer zonal wavenumber of the nth wave component of transient eddy forcing
$\omega_n \in [-2\pi, 2\pi] \times 5.787 \times 10^{-7}\ \mathrm{s^{-1}}$	Frequency of the nth wave component of transient eddy forcing
$\phi_n \in [0, 2\pi]$	Phase of the nth wave component of transient eddy forcing
$w_n \in [0, 3.7]$	Amplitude of the nth wave component of transient eddy forcing
$\Lambda \in [1, 18]\ \mathrm{m\,s^{-1}}$ (default = $10\ \mathrm{m\,s^{-1}}$)	Amplitude of stationary wave activity
$k \in [1, 10]$ (default = 2)	Zonal wavenumber of stationary wave activity
$\varepsilon \in [0.1, 2]$ (default = 0.5)	Nondimensional strength of stationary wave noise
$k_m \in [1, 10]$	Integer zonal wavenumber of the mth wave component of stationary wave noise
$\omega_m \in [-2\pi, 2\pi] \times 2.894 \times 10^{-7}\ \mathrm{s^{-1}}$	Frequency of the mth wave component of stationary wave noise
$\phi_m \in [0, 2\pi]$	Phase of the mth wave component of stationary wave noise
$w_m \in [0, 1]$	Amplitude of the mth wave component of stationary wave noise
Main control parameters	
$\gamma \in [0.5, 4]$	Strength of transient eddy forcing
$2\alpha\Lambda \in [1, 20]\ \mathrm{m\,s^{-1}}$	Stationary wave amplitude
$U_J \in [30, 90]\ \mathrm{m\,s^{-1}}$	Jet speed

In the subsequent experiments we will vary transient eddy forcing $\hat{S}(x, t)$, the amplitude of stationary wave $A_0(x)$ and the background group velocity $U_{\mathrm{REF}} + c_g$ in extended integrations of Eq. (1), and examine how the statistics of blocking responds to these "climate variations." We fix the other parameters as $\tau = 10$ days, $\alpha = 0.55$ and $\kappa = 3.26 \times 10^5\ \mathrm{m^2\,s^{-1}}$. The first two values are based on our previous observational analyses (Huang and Nakamura 2017; NH18), whereas the last value is consistent with Nakamura and Huang (2017). A periodic channel is assumed with a length of $L_x = 2.8 \times 10^7$ m. We have tested both finite-difference and spectral transform methods and obtained virtually identical results. The results shown in the next section are based on the spectral transform method with 1024 grid spacings. We use an exponential time differencing method with a fourth-order Runge–Kutta scheme (Cox and Matthews 2002; Kassam and Trefethen 2005) and a time increment of 432 s. We describe below the specific forms of the parameters to be varied. The list of parameters and the range of their values are found in Table 1.

a. Transient eddy forcing

Transient eddy forcing is prescribed through superposition of waves with different wavenumbers and frequencies:

$$\hat{S}_w(x,t) = \frac{\gamma}{N}\sum_{n=1}^{N} w_n \sin\left(\frac{2\pi k_n}{L_x}x + \omega_n t + \phi_n\right), \tag{5}$$

$$\hat{S}(x,t) = S_0 \max[1,\ 1 + \hat{S}_w^3(x,t)],$$
$$S_0 = 1.852 \times 10^{-5}\ (\mathrm{m\,s^{-2}}), \tag{6}$$

where γ controls the overall strength of forcing, and the variables with subscript n are picked randomly at the beginning of each simulation (and kept fixed during the simulation) with the following rules:

- The variable $N = 26$ and the zonal wavenumber of the component waves k_n is uniformly sampled from a set of integers between 1 and 20.
- Frequency of the component waves ω_n ($\mathrm{s^{-1}}$) is uniformly sampled from $[-2\pi, 2\pi] \times 5.787 \times 10^{-7}$.
- Phase of the component waves ϕ_n is uniformly sampled from $[0, 2\pi]$.
- Amplitude of the component waves w_n is uniformly sampled from [0, 3.7].

Constructive interference of waves in Eq. (5) gives rise to isolated "forcing events." To enhance the isolation, $\hat{S}_w(x, t)$ is raised to the third power and its minimum value is truncated at zero in $\hat{S}(x, t)$ [see Eq. (6)]. This will ensure that forcing is always above the positive baseline value S_0 specified in NH18 [their Eq. (S14)]. The above

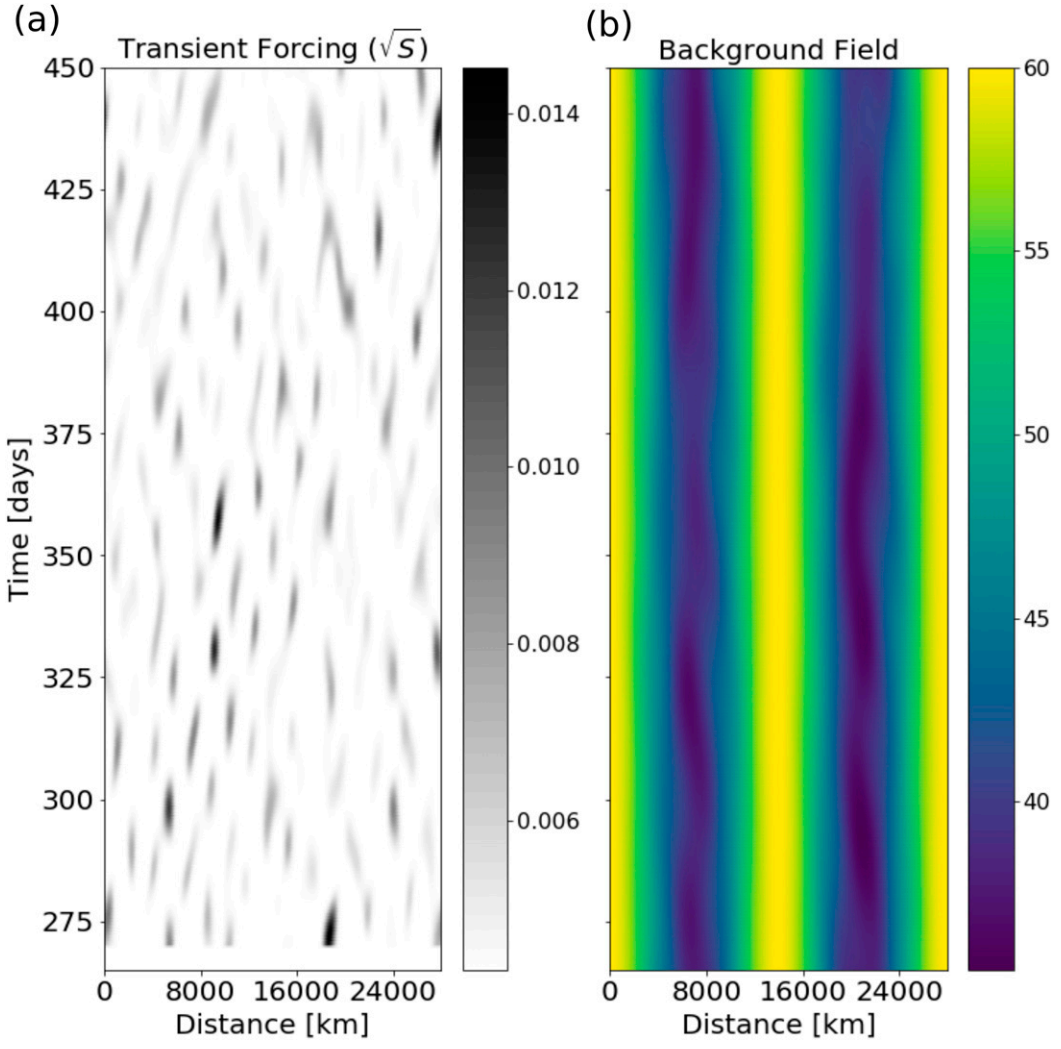

FIG. 1. (a) Example of transient eddy forcing $\hat{S}(x, t)$ with $\gamma = 2$. Horizontal axis is x (km) and vertical axis is t (days). Shades are scaled to $\hat{S}^{1/2}$. (b) As in (a), but for the background group velocity $C(x, t)$ with $U_{\mathrm{REF}} + c_g = 60\,\mathrm{m\,s^{-1}}$, $2\alpha\Lambda = 11\,\mathrm{m\,s^{-1}}$, $k = 2$, and $\varepsilon = 0.5$.

choice of parameters is determined by a trial-and-error method with the following guidelines: (i) forcing should be spectrally broad but limited to a range of wavenumbers and frequencies representative of synoptic events; (ii) within this spectral range, combination of the parameters should be randomized so that after many realizations a broad range of the forcing spectra is sampled. The purpose is to ensure that a robust blocking statistics emerges from a stochastic forcing, not from a narrowly prescribed frequency and length scale. Figure 1a shows a typical distribution of $\hat{S}(x, t)$ in a longitude–time (Hovmöller) diagram [the shades are scaled to the square root of $\hat{S}(x, t)$]. Forcing events are aperiodic and last for a few days. Some events are noticeably stronger than others and capable of triggering block formation, as we will see later. In the subsequent experiments we vary the strength of forcing through γ. For a given γ we repeat the simulation 240 times, each time randomizing the above phase parameters. In this sense the obtained ensemble of simulations is "pseudostochastic," even though Eq. (1) is deterministic.

b. *Stationary wave*

In NH18 "stationary wave" refers to the wave component that is time independent not only in phase but also in amplitude. It is defined as the minimum observed value of LWA at a given location. With this definition, amplification of stationary waves (in the traditional sense) by transient wave forcing becomes part of the transient wave dynamics. In what follows we slightly modify the definition in NH18 [their Eq. (S13)] to

$$A_0(x,t) = \Lambda\left[1 - \cos\left(\frac{2k\pi x}{L_x}\right)\right][1 + \mu(x,t)], \quad (7)$$

$$\mu(x,t) = \frac{\varepsilon}{M}\sum_{m=1}^{M} w_m \sin\left(\frac{2\pi k_m}{L_x} + \omega_m t + \phi_m\right), \quad (8)$$

where the zonal wavenumber k and noise-induced amplitude modulation μ are the additional degrees of freedom in the stationary wave. The latter is meant to mimic fluctuations in the stationary wave through boundary forcing. Similar to $\hat{S}_w(x, t)$ in Eq. (5), $\mu(x, t)$ is given in terms of superposition of interfering waves, where

- $M = 21$ and k_m is uniformly sampled from a set of integers between 1 and 10;
- ω_m is uniformly sampled from $[-2\pi, 2\pi] \times 2.894 \times 10^{-7}$ (s^{-1});
- ϕ_m is uniformly sampled from $[0, 2\pi]$;
- w_m is uniformly sampled from [0, 1].

The parameters with subscript m are randomized at the beginning of each simulation. The addition of the noise modifies $C(x)$ in Eq. (1) to $C(x, t) = U_{\mathrm{REF}} + c_g - 2\alpha A_0(x, t)$. Although the time dependence of A_0 may seem to obscure the distinction between stationary and transient waves, it represents a fundamentally distinct forcing process (boundary forcing as opposed to the internal dynamics) and operates at a slower time scale than the transient eddy forcing ($\omega_m < \omega_n$). We control the amplitude of the stationary wave through Λ and ε.

c. Jet speed

The sum $U_{\mathrm{REF}} + c_g$ denotes the average group velocity of Rossby waves in a hypothetical, wave-free reference state, including advection by the zonal wind U_{REF}. In a baroclinic atmosphere $U_{\mathrm{REF}}(y, z)$ would be inverted from the reference-state PV, $Q_{\mathrm{REF}}(y, z)$, which in turn would be obtained by zonalizing a wavy, instantaneous PV field through area-preserving map (Nakamura and Zhu 2010). In the absence of nonconservative processes U_{REF} would be invariant in time; in reality it varies slowly in response to diabatic heating, mixing, frictional damping, etc., and shows large seasonal variation (Nakamura and Solomon 2010, 2011; Methven and Berrisford 2015). Since we are concerned with blocking statistics under a characteristic flow condition, we prescribe $U_{\mathrm{REF}} + c_g$ as a constant for each simulation. Figure 4 of NH18 (orange diamonds) indicates that the background group velocity is nearly constant over a wide range of LWA. Its variation primarily represents changes in the jet speed U_{REF} in response to seasonal to decadal climate forcing. The change in the background PV gradient can also affect c_g, but in the storm-track regions the magnitude of c_g is generally much smaller than U_{REF} (not shown) and so the latter effect is thought to be minor. For this reason, we will subsequently refer to $U_{\mathrm{REF}} + c_g \equiv U_J$ as "jet speed."

Figure 1b shows a typical structure of $C(x, t)$ for $U_J = 60\,\mathrm{m\,s^{-1}}$, $\Lambda = 10\,\mathrm{m\,s^{-1}}$, $k = 2$, and $\varepsilon = 0.5$. The predominant stationary wavenumber 2 creates two minima in $C(x, t)$, while the effect of noise is minimal with this parameter choice.

d. Nondimensional parameters

Although in the subsequent experiments we vary the above three parameters in dimensional forms, it is instructive to see how they relate to the nondimensional parameters of Eq. (1). If we nondimensionalize x and t by L_x and $L_x U_J^{-1}$, respectively, and $\hat{A}$ and C with U_J, the following five nondimensional parameters emerge:

$$a_1 = 2\alpha\Lambda(1+\varepsilon)U_J^{-1}, \quad a_2 = k, \quad a_3 = S_0 L_x(1+\gamma^3)U_J^{-2},$$
$$a_4 = L_x(\tau U_J)^{-1}, \quad a_5 = \kappa(L_x U_J)^{-1}. \quad (9)$$

Here, a_1 and a_2 measure the magnitude and wavenumber of stationary wave activity; a_3 is the magnitude of transient eddy forcing; a_4 and a_5 quantify the strengths of damping and diffusion. We fix L_x, α, S_0, τ, and κ in all of the subsequent experiments (and ε and k for most experiments), but U_J affects all but one of the parameters when we vary the jet speed. For an intuitive interpretation, in what follows we characterize our results with the three (dimensional) parameters, $2\alpha\Lambda$, γ, and U_J, instead of the above nondimensional parameters. Again see Table 1 for the list of parameters.

3. Results

The above model is used to simulate block formation in extended runs. For each run, we choose a combination of $2\alpha\Lambda$, γ, and U_J, and randomize the phase parameters of transient eddy forcing and stationary wave noise. The model is run for 270 days without the transient eddy forcing or stationary wave noise to reach a steady state, at which point we switch on the transient forcing and noise. Subsequently the model is run for another 180 days and we identify blocking events by the detection algorithm described below. We repeat the transient part of experiment 240 times for the same combination of $2\alpha\Lambda$, γ, and U_J, each time randomizing the phase parameters. We write out the snapshot of LWA to the disk at every 50 time steps (36 min) for postprocessing.

a. Illustrative results

Figure 2 illustrates solutions for two representative flow regimes in Hovmöller diagrams. The first three

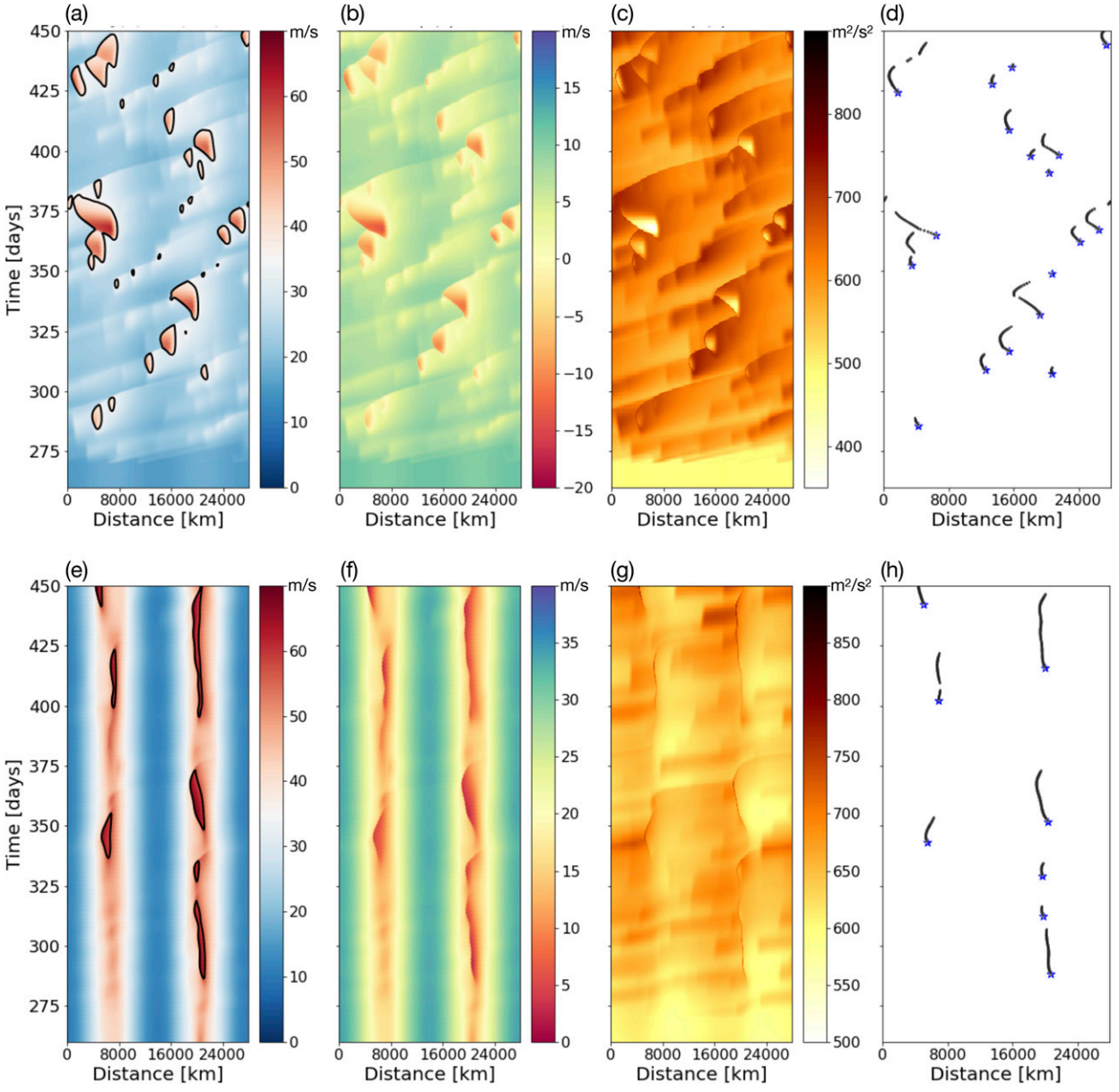

FIG. 2. Sample solutions of Eq. (1) as functions of longitude x (km) and time t (days). (a)–(d) $2\alpha\Lambda = 0.8\,\mathrm{m\,s^{-1}}$, $\gamma = 3$, $U_J = 40\,\mathrm{m\,s^{-1}}$, $k = 2$, $\varepsilon = 0.5$. The corresponding nondimensional parameters [Eq. (9)] are $(a_1, a_2, a_3, a_4, a_5) = (0.03, 2, 9.1, 0.81, 0.000\,29)$. (e)–(h) $2\alpha\Lambda = 11\,\mathrm{m\,s^{-1}}$, $\gamma = 2$, $U_J = 60\,\mathrm{m\,s^{-1}}$, $k = 2$, $\varepsilon = 0.5$, or $(a_1, a_2, a_3, a_4, a_5) = (0.28, 2, 1.3, 0.54, 0.000\,19)$. (a),(e) Total wave activity $A(x, t) = A_0(x) + \hat{A}(x, t)$ $(\mathrm{m\,s^{-1}})$. In the areas enclosed by the black contours the wave activity exceeds the threshold value: $\hat{A} > \hat{A}_c$ [Eq. (4)]. (b),(f) Zonal wind $u(x, t) \equiv 40 - \alpha A(x, t)$ $(\mathrm{m\,s^{-1}})$. (c),(g) Zonal flux of transient LWA $F = [C(x) - \alpha\hat{A}]\hat{A}$ $(\mathrm{m^2\,s^{-2}})$. (d),(g) Binary mask used to identify blocks. The stars indicate the first pixel in each block. See text for details.

panels in the top row show the total LWA, $A = A_0 + \hat{A}$ (Figs. 2a), zonal wind, $u \equiv 40 - \alpha A$ (Figs. 2b), and the transient LWA flux F (Figs. 2c) for a weak stationary wave forcing ($2\alpha\Lambda = 0.8\,\mathrm{m\,s^{-1}}$, $\gamma = 3$, $U_J = 40\,\mathrm{m\,s^{-1}}$, $k = 2$, and $\varepsilon = 0.5$). In this case, transient eddy forcing generates a series of wave packets that migrate downstream, characterized by diagonal stripes in all variables. Due to the imposed damping ($\tau = 10$ days) the packets have finite lengths, and the LWA flux (Fig. 2c) is approximately proportional to LWA (Fig. 2a). Occasionally strong forcing events cause the threshold [Eq. (4)] to be exceeded, indicated by black contours in Fig. 2a. The majority of these supercritical episodes are short-lived and minor, and they occur throughout the channel, as they are a direct response to the forcing events. In this particular realization, a few significant episodes occur in

the upstream of the weak stationary LWA ridges with substantial accumulation of LWA (Fig. 2a), deceleration of zonal wind (Fig. 2b) and precipitous drop in the LWA flux (Fig. 2c), but these episodes are generally infrequent in this parameter setting.

The bottom row (Figs. 2e–g) shows a case with stronger stationary wave and faster jet ($2\alpha\Lambda = 11\,\mathrm{m\,s^{-1}}$, $\gamma = 2$, $U_J = 60\,\mathrm{m\,s^{-1}}$, $k = 2$, and $\varepsilon = 0.5$). The model climate in this case is dominated by persistent anomalies in all variables. Although forcing events are patchy and spread over the entire domain (Fig. 1a), regions that exceed the threshold form and persist primarily in the vicinity, and slightly upstream, of the stationary LWA ridges where the zonal wind is perpetually weak. Large-amplitude anomalies coincide with these regions, and they have sharp, shock-like upstream edges (Nakamura and Huang 2017), at which the downstream LWA flux is disrupted abruptly (Figs. 2e–g). Anomalies grow by expanding the upstream edges westward by absorbing the incident LWA flux (Figs. 2e,f) before they die out. That this case produces persistent anomalies despite the much weaker transient eddy forcing than the previous case ($a_3 = 1.3$ as opposed to 9.1) highlights the importance of stationary wave and the associated streamwise variation in the wind speed in producing and localizing the persistent anomalies. We will present a more comprehensive parameter sweep shortly.

b. Detection method and metrics

To construct statistics of blocking, one needs a method to identify and count the blocking episodes. In designing a detection method, we considered two criteria: (i) a blocking event should be roughly bounded by the threshold condition [Eq. (4)] but also reflect some maturity; (ii) instead of defining a block by an arbitrary minimum duration, we wish to obtain a distribution of frequency and persistence of episodes. In the end, the following method has been adopted, along with three metrics of blocks: (i) frequency, (ii) prevalence, and (iii) persistence. We first identify the grids in the longitude–time domain of the experiment ($L_x \times 180$ days) at which the magnitude of $\partial u/\partial x$ (or equivalently $\partial A/\partial x$) exceeds five standard deviations. They typically coincide with the upstream edges of blocking episodes.[2] Next we apply a binary mask, namely, assign a value of 1 to these grids and 0 everywhere else. We will then run a counting algorithm outlined in appendix B, which identifies a single grid at the onset of each blocking episode. We count these grids in the domain to determine the *frequency* of blocks. To measure the overall *prevalence* of blocks, we count the total number of the grids with the value of 1 in the domain (blocking pixels). We then evaluate the average *persistence* of individual blocks by dividing prevalence by the number of blocks in the domain.

Figures 2d and 2h show the blocking pixels (wiggly strings) and the onset grids (stars) for the two experiments with weak and strong stationary wave forcing. Even though the former identifies many more blocks (18 vs 8), most of them have short persistence.

c. Parameter sweep

Figure 3 summarizes the result of parameter sweep experiments. Each column describes the response of blocking statistics to the variation of one parameter, using the three metrics introduced above. In the left column, we vary the stationary wave amplitude $2\alpha\Lambda$ with the other parameters fixed at default values (see the figure caption). When the stationary wave is weak, blocks are either rare or short-lived, so the prevalence is small. Both prevalence and frequency increase sharply as the stationary wave amplitude is increased beyond $2\alpha\Lambda \sim 10\,\mathrm{m\,s^{-1}}$ (Figs. 3a,b), as the threshold [Eq. (4)] is fulfilled more frequently. Although the variation of prevalence is monotonic, frequency decreases some as the stationary wave amplitude is raised further (Fig. 3b). This is because blocks merge and become more persistent, as revealed in Fig. 3c. Frequency also exhibits greater uncertainty than prevalence partly due to its discrete nature (mostly single-digit integers). The uncertainty in frequency also causes uncertainty in persistence.

In the second column, we increase transient eddy forcing eightfold. In response, prevalence increases monotonically by a factor of 2 or so (Fig. 3d). Frequency averages around 6 $(180\ \mathrm{days})^{-1}$ when forcing is weak, and it increases slightly with forcing. For stronger forcing, however, frequency decreases significantly despite the continued increase in prevalence (Fig. 3e). This is due to a marked increase in persistence, by a factor of 3 over the range of forcing examined (Fig. 3f). Figure 4 is similar to the bottom row of Fig. 2 but with a stronger eddy forcing. In this case blocking becomes nearly perpetual in the vicinity of the two stationary ridges in LWA (Fig. 4d), and the zonal wind and flux often reverse to westward (Figs. 4b,c).

The response of blocking to the jet speed variation is roughly the opposite of the response to the stationary wave amplitude (Fig. 3, right column): prevalence and frequency decrease sharply beyond $U_J \approx 60\,\mathrm{m\,s^{-1}}$

[2] We have also tried other criteria, including the convergence of the LWA flux and $\log_{10}(1 - \Gamma)$ [Eq. (4)]. They produce slightly different blocking counts but have similar dependence on the model parameters.

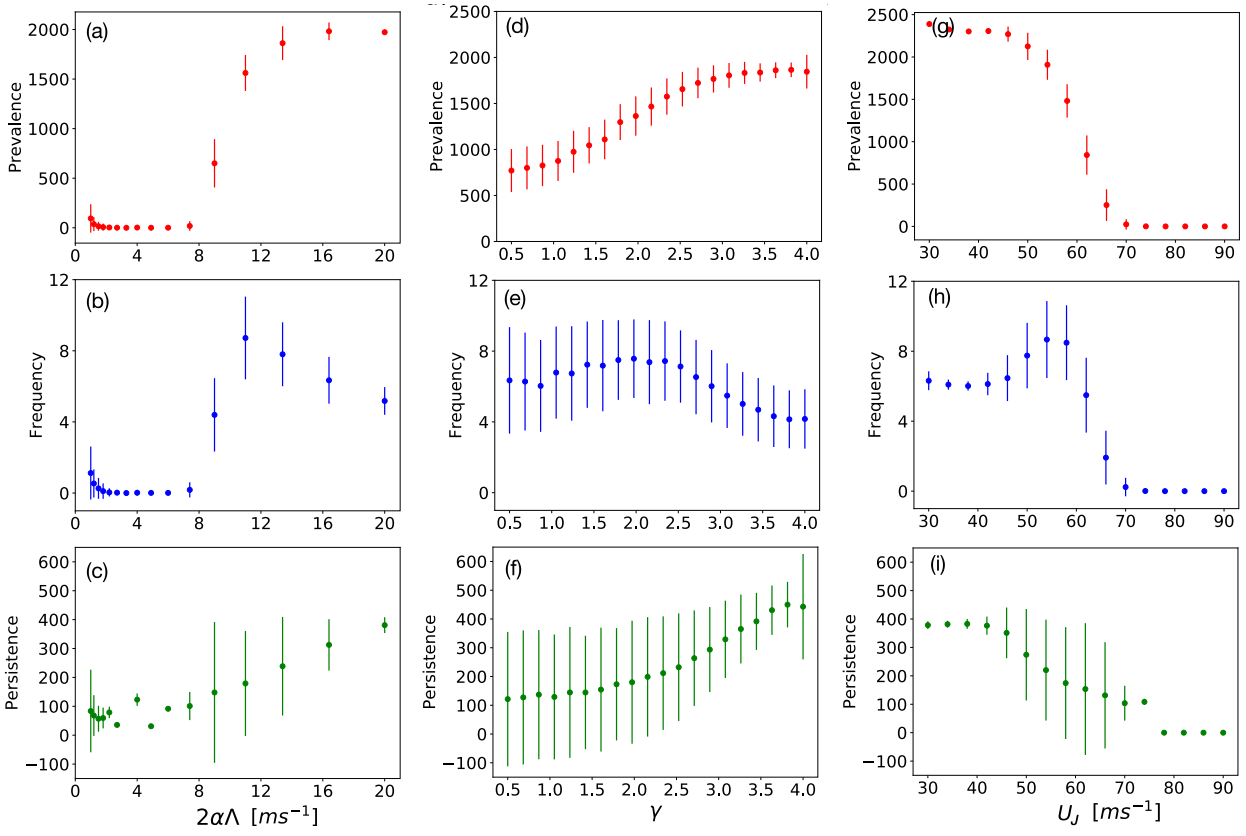

FIG. 3. Response of blocking metrics (rows) to the variation of model parameters (columns). (top) Prevalence (total number of blocking pixels over 180 days). (middle) Frequency (number of blocks per 180 days). (bottom) Persistence (average number of blocking pixels per event). To convert to days, multiply by 0.025. (a)–(c) Stationary wave amplitude $2\alpha\Lambda$ ($\mathrm{m\,s^{-1}}$), with $k = 2$, $\varepsilon = 0.5$, $\gamma = 2$, $U_J = 60\,\mathrm{m\,s^{-1}}$. (d)–(f) Transient eddy forcing amplitude γ, with $2\alpha\Lambda = 11\,\mathrm{m\,s^{-1}}$, $k = 2$, $\varepsilon = 0.5$, $U_J = 60\,\mathrm{m\,s^{-1}}$. (g)–(i) Jet speed U_J ($\mathrm{m\,s^{-1}}$), with $2\alpha\Lambda = 11\,\mathrm{m\,s^{-1}}$, $k = 2$, $\varepsilon = 0.5$, $\gamma = 2$. For each parameter combination, statistics are computed from a 240-member ensemble. Error bars indicate plus and minus one standard deviation. See text for details.

(Figs. 3g,h). This is understandable since increasing the jet speed has the same effect as decreasing the stationary wave amplitude in a_1 [Eq. (9)]. However, in the limit of slow jet speed, prevalence is significantly higher than in the limit of large stationary wave amplitude (Fig. 3g vs Fig. 3a). This is because the decreasing jet speed effectively increases transient eddy forcing a_3 relative to damping and diffusion terms a_4 and a_5 [Eq. (9)]. Persistence also decreases, albeit more slowly, until $U_J \approx 75\,\mathrm{m\,s^{-1}}$, beyond which blocks virtually disappear (Fig. 3i).

Figure 5 summarizes the blocking statistics as functions of stationary wave amplitude and jet speed. All three metrics show clear transition from a nearly block-free state to a block-dominant state. When the jet is slow, this transition occurs at small stationary wave amplitude. As the jet speed increases, larger stationary wave amplitude is required for the transition. A slight exception to this rule is frequency at small stationary wave amplitude, which shows weak secondary maximum along the vertical axis (Fig. 5b). This is because when the stationary wave is weak and eddy forcing is reasonably strong, blocks with short persistence arising directly from forcing prevail (see Fig. 2d).

We have also tested the parameter dependence in the context of an initial-value problem. Figure 6 shows the result of a 145-yr run, in which the jet speed U_J is decreased gradually from $70\,\mathrm{m\,s^{-1}}$ at a rate of $0.17\,\mathrm{m\,s^{-1}\,yr^{-1}}$, while other parameters are fixed ($2\alpha\Lambda = 11\,\mathrm{m\,s^{-1}}$, $\gamma = 2$, $k = 2$, $\varepsilon = 0.5$). In this case we have randomized the phase of the forcing at certain intervals to avoid inadvertent periodicity. Each panel shows the total LWA $A_0 + \hat{A}$ for a 250-day period, 5 years apart. During the first 40 years, the jet speed decreases by about 10% but both the frequency and persistence of the episodes that exceed the threshold (roughly equal to blocks) remain low. However, between year 40 and 80, approximately the same amount of jet speed reduction brings about a rapid increase in the persistence of blocking events. Further reduction of the jet speed in the subsequent years causes the blocks to

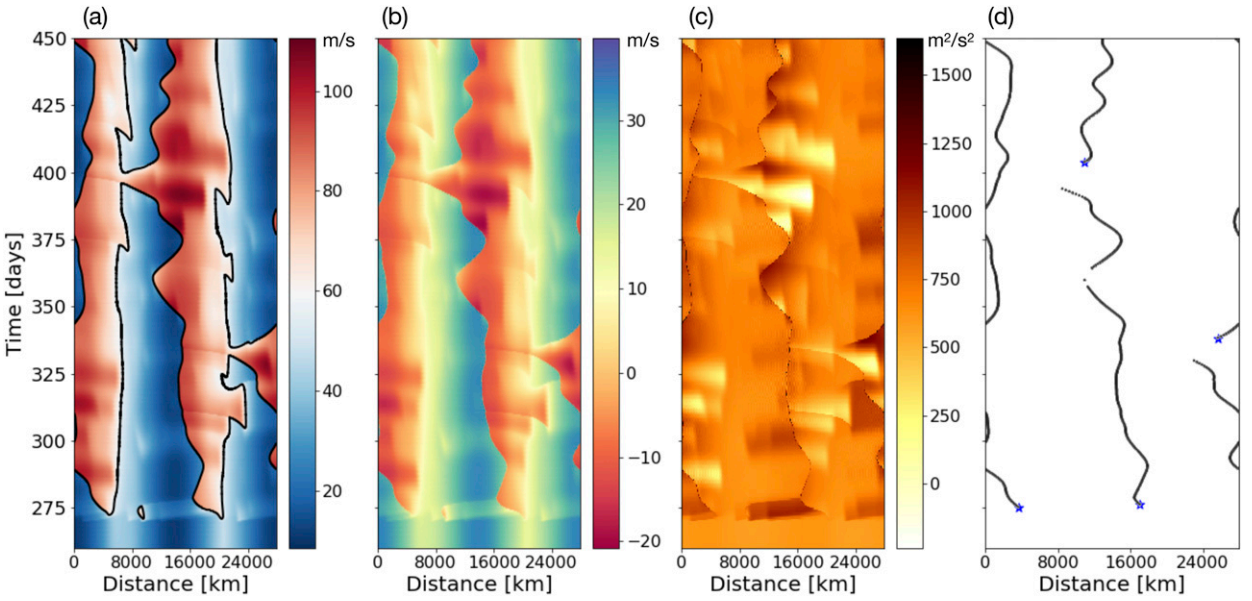

FIG. 4. As in Figs. 2e–h, but for $\gamma = 4$, or $(a_1, a_2, a_3, a_4, a_5) = (0.28, 2, 9.4, 0.54, 0.000\,19)$.

remain quasi perpetual and its zonal extent to expand upstream. While the result is consistent with Fig. 5, we stress that this is a hypothetical exercise, in which only the jet speed is varied. Although the ongoing Arctic amplification potentially leads to a long-term reduction in the jet speed (Francis et al. 2017), it is doubtful that this parameter remains independent of other parameters such as transient eddy forcing under the real climate change.

d. Dependence on other parameters

In addition to the three parameters, we have also varied the wavenumber k [Eq. (7)] and the noise level ε [Eq. (8)] of the stationary wave. When the wavenumber of stationary wave is increased from 1 to 10, prevalence dips initially ($1 \leq k \leq 3$) and then turns upward (Fig. 7a). However, the overall variation of prevalence is modest (the maximum at $k = 10$ is only 33% above the minimum at $k = 3$). Frequency, on the other hand, shows a nearly linear, threefold increase over $1 \leq k \leq 10$ (Fig. 7b). This is because the increasing wavenumber adds more stationary ridges in LWA that are traffic bottlenecks and conducive to blocking. However, since prevalence does not change much, blocks become more numerous but shorter. Persistence decreases by about 50% over $1 \leq k \leq 4$ although the subsequent reduction is very modest (Fig. 7c). Overall, the wavenumber of the stationary wave affects the frequency (and locations) of blocking the most.

When we increase the noise level of the stationary wave amplitude ε, both prevalence and frequency increase rapidly at first and gradually level off as ε increases further. Persistence, on the other hand, remains more or less steady (Figs. 7d–f). Comparisons with Figs. 3a, 3b, and 5 suggest that the enhanced ε effectively increases the amplitude of stationary wave and accelerates the transition from the block-free state to the block-dominant

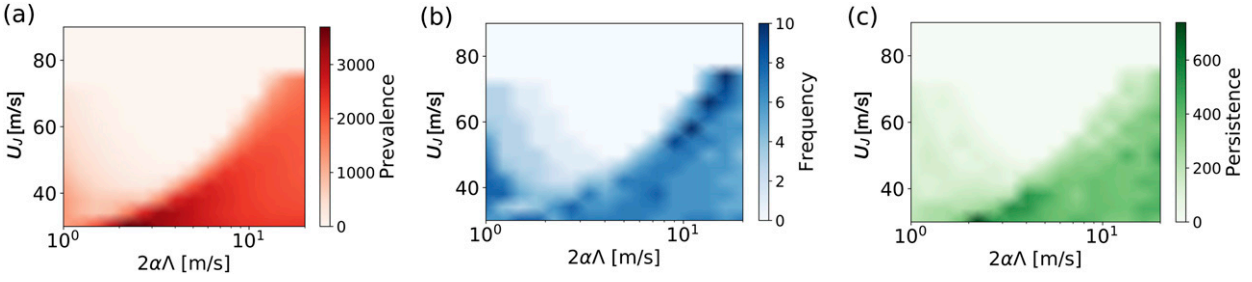

FIG. 5. Dependence of blocking metrics on stationary wave amplitude $2\alpha\Lambda$ (horizontal axis; m s^{-1}) and U_J (vertical axis; m s^{-1}). Note the logarithmic scale of the abscissa: (a) prevalence, (b) frequency, and (c) persistence. Other parameters are fixed as $\gamma = 2$, $k = 2$, and $\varepsilon = 0.5$.

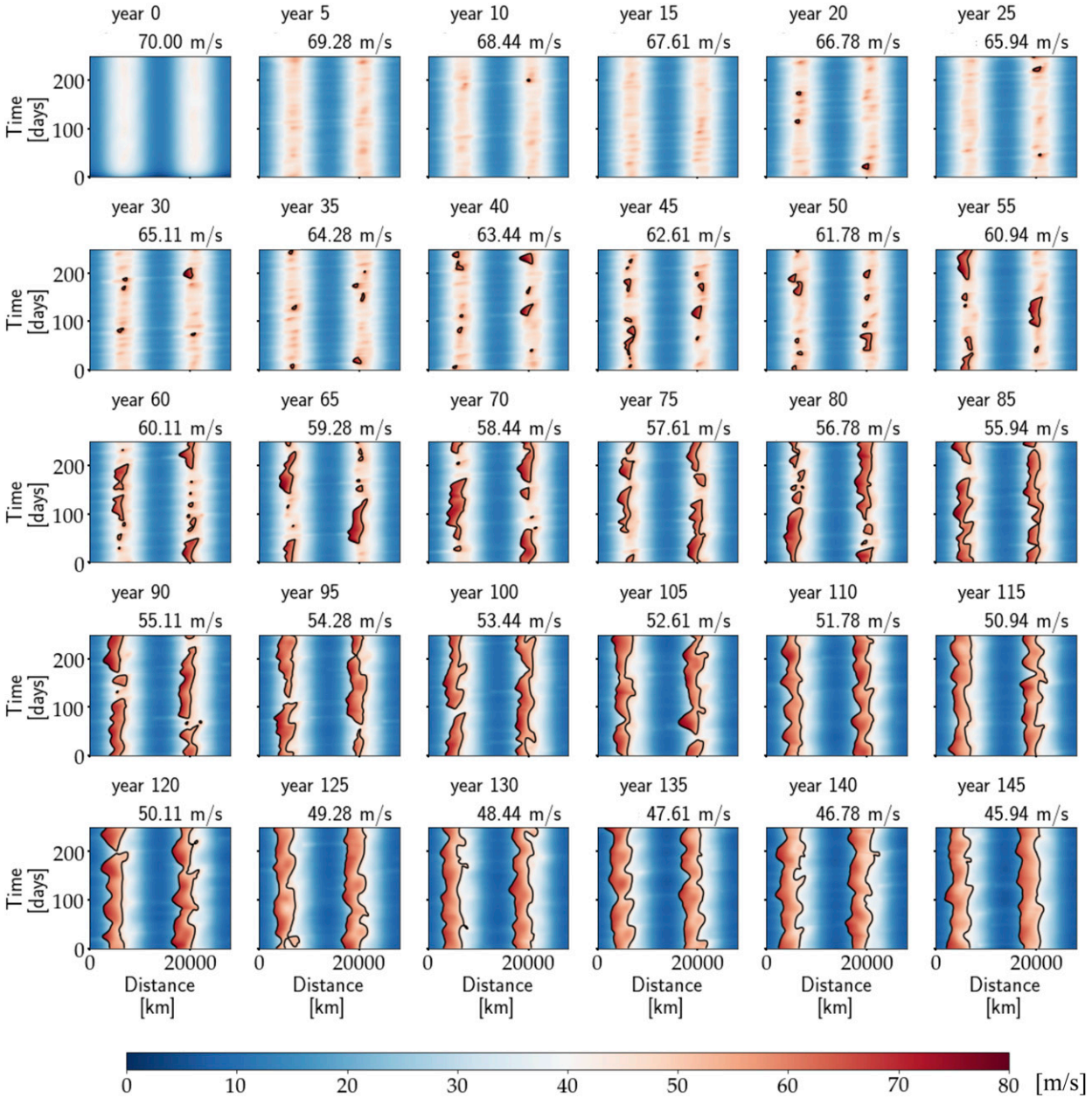

FIG. 6. Total wave activity in a long-term simulation (from year 0 to 145), in which U_J is decreased from 70 m s^{-1} at a rate of 0.17 m s^{-1} yr^{-1}, while we fix $2\alpha\Lambda = 11$ m s^{-1}, $\gamma = 2$, $k = 2$, and $\varepsilon = 0.5$. Each panel shows 250 days of snapshots 5 years apart. The value of U_J averaged over the 250-day period is shown above each panel. The transient eddy forcing is introduced after year 0 and is not reflected in the top-left panel. Other conventions are as in Figs. 2a and 2e. See text for details.

state, greatly affecting the frequency and prevalence in the transition zone.

4. Summary and discussion

Current climate models do not exhibit high confidence in the projection of blocking frequency under a changing climate (Woollings et al. 2018). Even discounting the systematic biases and other shortcomings of the model simulations, building reliable statistics of blocking events, let alone evaluating the nonstationary aspect of it, is inherently resource intensive due to the intermittent nature of blocks. Given this, there is a virtue in studying blocking statistics using a simple model that grants computational economy and theoretical interpretations.

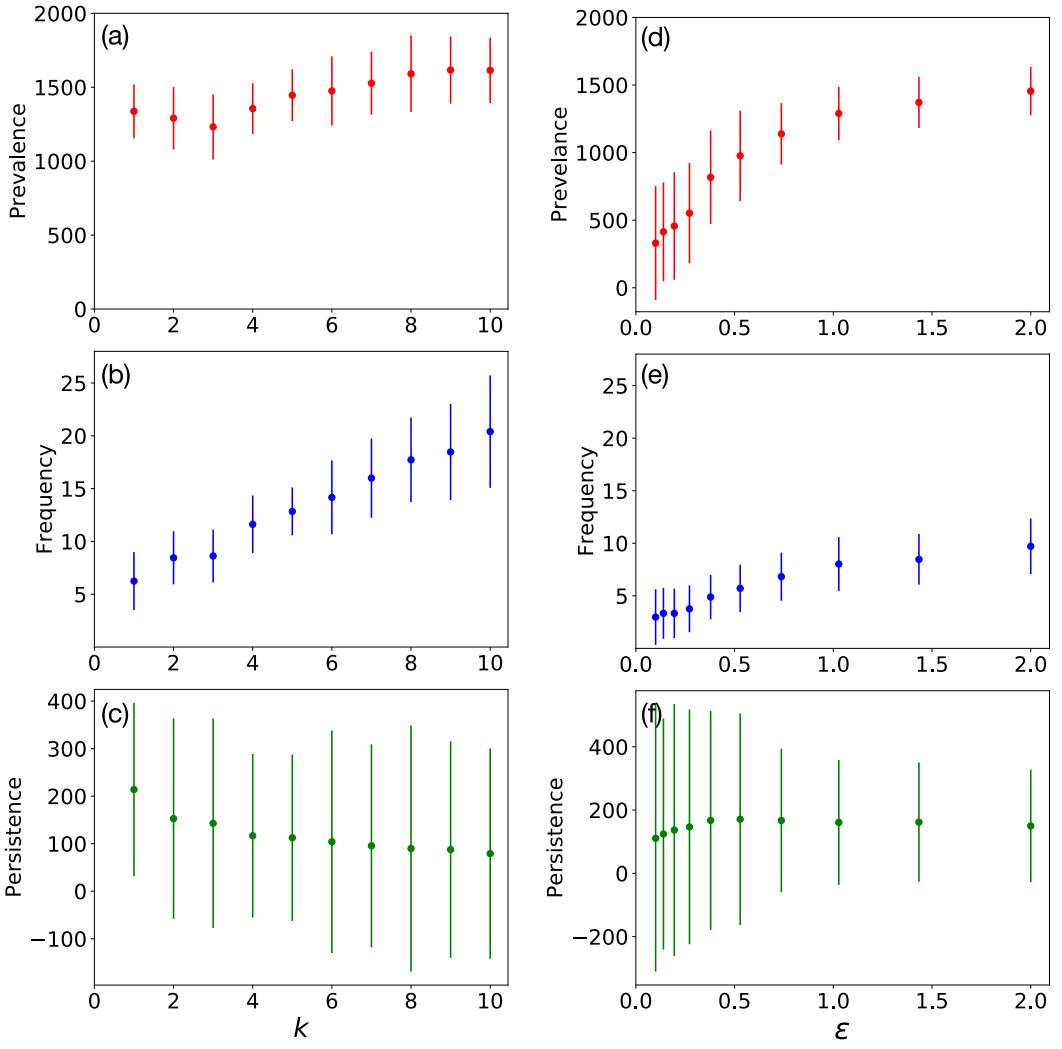

FIG. 7. Response of blocking metrics to the variation of wavenumber of (a)–(c) stationary wave k and (d)–(f) noise level of the stationary wave amplitude ε for (top) prevalence, (middle) frequency, and (bottom) persistence. Other parameters are fixed as $2\alpha\Lambda = 11\,\mathrm{m\,s^{-1}}$, $U_J = 60\,\mathrm{m\,s^{-1}}$, $\gamma = 2$, $k = 2$, and $\varepsilon = 0.5$. See text for details.

We have constructed and analyzed a large ensemble of 180-day simulations in the parameter space of the "traffic jam" model of blocking [NH18; Eq. (1)]. In this simple 1D model, transient waves are generated by pseudostochastic eddy forcing and allowed to interact with the westerly wind and stationary wave. Although the statistics of transient eddy forcing is homogeneous, blocks form by selectively collecting the wave activity flux from significant forcing events in the upstream of the stationary LWA ridge. The majority of blocks in this model therefore form in the vicinity (or slightly upstream) of the stationary LWA ridges, where the westerly wind is always weak. This matches the climatological locations of the major blocks in the Northern Hemisphere, which center around the exit regions of the storm tracks (Woollings et al. 2018). The boundaries of blocks generally coincide well with the threshold condition [Eq. (4)]. Therefore, the modulations of the threshold condition due to changes in the parameters (climate variations) affect the blocking statistics.

Blocking statistics in this model proves particularly sensitive to the stationary wave amplitude and the jet speed. For a given transient eddy forcing, the model's climate shifts quickly from a block-free state to a block-dominant state as the stationary wave amplitude is increased and/or the jet speed is reduced. Proximity to the blocking threshold is determined by the ratio of LWA to the jet speed. As the stationary wave LWA increases, less additional transient wave LWA is required to fulfill the threshold. As a result, a greater stationary wave is more conducive to block formation for the given jet speed and transient eddy forcing. Similarly, a slower jet

makes the flow closer to the threshold and thus more conducive to block formation for the given stationary wave and transient eddy forcing.

An increasing transient eddy forcing also promotes blocking, and its main effect in the presence of stationary waves is to make blocking fewer and more persistent (and eventually perpetual). Causes of transient eddy forcing include baroclinic cyclogenesis in the upstream (Colucci 1985), diabatic heating associated with moist processes (Pfahl et al. 2015), and merger of storms (Riboldi et al. 2019). Given that we observe blocks frequently but not perpetually in the real atmosphere, we speculate that the present climate lies close to the transition between block-free and block-dominant states. Furthermore, we envision that the seasonal variation (strong stationary waves and a fast jet in winter; weak stationary waves and a slower jet in summer) moves the state of the atmosphere along, but not across, the regime boundary, so blocking is observed year-round. Since the boundary is sharp with respect to the stationary wave amplitude and jet speed, blocking in climate models is likely sensitive to these quantities if the present climate indeed lies in the vicinity of the regime boundary. Many CMIP5 models underestimate the frequency of Atlantic blocking, and even though they collectively predict a weak decreasing trend in future blocking frequency, the confidence level of the projections is low (Masato et al. 2013; Woollings et al. 2018). A positive bias in the jet speed and/or a negative bias in the stationary wave amplitude are the prime candidates that suppress the Atlantic blocks in these models. If these biases in large-scale circulation patterns can be corrected, blocking statistics in the climate models may improve significantly (Scaife et al. 2011). However, the cause of the biases is nontrivial: for example, poor resolution of orography and moist convection affects the stationary wave amplitude, and inadequate representation of sea surface temperature affects the overall mean states of the storm tracks (Berckmans et al. 2013). Because of the intricate interplay among the internal processes, correcting for the bias requires a careful and holistic examination of the model dynamics. Understanding how flow parameters influence various aspects of blocking is just the starting point; it provides a theoretical framework for addressing the model biases, as well as interpreting the observed trends in blocking statistics.

Given the highly idealized nature of Eq. (1), some details of the blocking dynamics it represents merit further scrutiny. In particular, the demise phase of blocking likely involves meridional transmission of Rossby wave packets, and expressing it as linear damping with a constant damping time scale is a gross oversimplification. How a more elaborate representation of wave activity fluxes affects the persistence of blocks is a topic worthy of future study.

In this work we focused on the local interaction between transient waves and zonal flow as a mechanism of block formation, wherein the stationary wave amplitude was prescribed. A complementary mechanism of block formation is resonance between the boundary forcing and stationary waves (Charney and DeVore 1979; Tung and Lindzen 1979; Brunet 1994; Petoukhov et al. 2013). While resonance is discussed primarily in the context of amplification of the stationary wave, our study suggests that an enhanced stationary wave can in turn affect blocking through interaction with transient waves, by modulating the threshold. This is implied in section 3, where perturbation to the stationary wave resulted in a significant change in the blocking statistics. Relative importance of the traffic jam and resonance dynamics will be investigated in subsequent works.

Acknowledgments. The main results of this paper emerged from a group project during *Rossbypalooza*, a student-led summer school at the University of Chicago in June 2018, with the theme of ''Understanding climate through simple models.'' The authors thank the participants of the summer school for their valuable feedback. Constructive criticisms of the two anonymous reviewers greatly improved the quality of the manuscript. The work is supported by NSF Grants AGS1563307 and AGS1810964.

APPENDIX A

The Diffusive Term in Eq. (1)

Here we demonstrate that the last term in Eq. (1) may be linked to the correlation between PV and zonal wind along the meridional path of displacement. In the horizontal Cartesian plane the zonal advective flux of LWA takes the form (Huang and Nakamura 2016)

$$U_{\mathrm{REF}}(y)A(x,y,t) - \int_0^{\eta(x,y,t)} u_e q_e \, dy', \tag{A1}$$

where

$$A(x,y,t) = -\int_0^{\eta(x,y,t)} q_e(x, y+y', t)\, dy' \tag{A2}$$

is LWA and

$$\begin{aligned} q_e(x,y+y',t) &= q(x,y+y',t) - Q_{\mathrm{REF}}(y) \\ u_e(x,y+y',t) &= u(x,y+y',t) - U_{\mathrm{REF}}(y) \end{aligned} \tag{A3}$$

denote PV and zonal wind along the meridional displacement coordinate y' relative to the wave-free reference state at y, and $y + \eta(x, y, t)$ is the instantaneous meridional location of the PV contour $q = Q_{\mathrm{REF}}$ at x [i.e. $q_e(x, y + \eta, t) = 0$]. Now define the average along the displacement path and departure from it as

$$\langle(\cdot)\rangle \equiv \frac{1}{\eta(x,y,t)}\int_0^{\eta(x,y,t)} (\cdot)\, dy', \quad (\cdot)^\dagger \equiv (\cdot) - \langle(\cdot)\rangle. \tag{A4}$$

Then $A = -\eta\langle q_e\rangle$ and Eq. (A1) may be rewritten as

$$(U_{\mathrm{REF}} + \langle u_e\rangle)A - \int_0^{\eta(x,y,t)} u_e^\dagger q_e^\dagger\, dy'. \tag{A5}$$

Introducing zonal displacement of fluid parcel relative to the meridional line of displacement, $\xi^\dagger(x, y + y', t)$, such that

$$u_e^\dagger = D\xi^\dagger/Dt, \quad q_e^\dagger \approx -\xi^\dagger \partial\langle q_e\rangle/\partial x, \tag{A6}$$

then Eq. (A5) becomes

$$(U_{\mathrm{REF}} + \langle u_e\rangle)A - \frac{\partial A}{\partial x}\left\langle \frac{D\xi^\dagger}{Dt}\xi^\dagger \right\rangle. \tag{A7}$$

If we let

$$\kappa \equiv \left\langle \frac{D\xi^\dagger}{Dt}\xi^\dagger \right\rangle, \tag{A8}$$

the last term in Eq. (A7) becomes a diffusive flux of LWA as long as $\kappa > 0$, giving rise to the diffusive term in Eq. (1). In deriving Eq. (1), we also assumed $\langle u_e\rangle \approx -\alpha A$.

APPENDIX B

Counting of Discrete Patches

We implement a simple algorithm inspired by the classical computation problem, the Game of Life (Gardner 1970), to count discrete patches in a 2D domain. We assume that the 2D field is binary, that is, every grid point is assigned a value of either 0 or 1. We will count the number of contiguous areas represented by the grid points with 1. To do this, we scan the entire domain using a five-point stencil $[(i, j), (i + 1, j), (i - 1, j), (i, j + 1), (i, j - 1)]$, where i and j are the indices of grids in the domain. In our case, the scan is performed along the row from top down, starting from the highest j to the lowest j (i.e., backward in time, forward in longitude). As we move the stencil across the domain, if the grid (i, j) has a value of 1, we check the values at the neighboring four grids. If any other grid has a value of 1, the value at (i, j) is reset to 0. This means that when the stencil reaches the last grid in a patch, only one grid is left from that patch with a value of 1. Once the stencil has reached the end of the domain, we sum the value of the entire grid. Since we now have one grid with a value of 1 per patch and 0 everywhere else, this sum is the number of patches. See the animation in the supplemental material.

REFERENCES

Altenhoff, A., O. Martius, M. Croci-Maspoli, C. Schwierz, and H. Davies, 2008: Linkage of atmospheric blocks and synoptic-scale Rossby waves: A climatological analysis. *Tellus*, **60A**, 1053–1063, https://doi.org/10.1111/j.1600-0870.2008.00354.x.

Barnes, E., J. Slingo, and T. Woollings, 2012: A methodology for the comparison of blocking climatologies across indices, models and climate scenarios. *Climate Dyn.*, **38**, 2467–2481, https://doi.org/10.1007/s00382-011-1243-6.

——, E. Dunn-Sigouin, G. Masato, and T. Woollings, 2014: Exploring recent trends in northern hemisphere blocking. *Geophys. Res. Lett.*, **41**, 638–644, https://doi.org/10.1002/2013GL058745.

Berckmans, J., T. Woollings, M. Demory, P.-L. Vidale, and M. Roberts, 2013: Atmospheric blocking in a high resolution climate model: Influences of mean state, orography and eddy forcing. *Atmos. Sci. Lett.*, **14**, 34–40, https://doi.org/10.1002/asl2.412.

Brunet, G., 1994: Empirical normal mode analysis of atmospheric data. *J. Atmos. Sci.*, **51**, 932–952, https://doi.org/10.1175/1520-0469(1994)051<0932:ENMAOA>2.0.CO;2.

Butchart, N., K. Haines, and J. C. Marshall, 1989: A theoretical and diagnostic study of solitary waves and atmospheric blocking. *J. Atmos. Sci.*, **46**, 2063–2078, https://doi.org/10.1175/1520-0469(1989)046<2063:ATADSO>2.0.CO;2.

Cash, B., and S. Lee, 2000: Dynamical processes of block evolution. *J. Atmos. Sci.*, **57**, 3202–3218, https://doi.org/10.1175/1520-0469(2000)057<3202:DPOBE>2.0.CO;2.

Charney, J., and J. DeVore, 1979: Multiple flow equilibria in the atmosphere and blocking. *J. Atmos. Sci.*, **36**, 1205–1216, https://doi.org/10.1175/1520-0469(1979)036<1205:MFEITA>2.0.CO;2.

Colucci, S., 1985: Explosive cyclogenesis and large-scale circulation changes: Implications for atmospheric blocking. *J. Atmos. Sci.*, **42**, 2701–2717, https://doi.org/10.1175/1520-0469(1985)042<2701:ECALSC>2.0.CO;2.

——, 2001: Planetary-scale preconditioning for the onset of blocking. *J. Atmos. Sci.*, **58**, 933–942, https://doi.org/10.1175/1520-0469(2001)058<0933:PSPFTO>2.0.CO;2.

Cox, S. M., and P. C. Matthews, 2002: Exponential time differencing for stiff systems. *J. Comput. Phys.*, **176**, 430–455, https://doi.org/10.1006/jcph.2002.6995.

Francis, J. A., S. Vavrus, and J. Cohen, 2017: Amplified arctic warming and mid-latitude weather: New perspectives on emerging connections. *Wiley Interdiscip. Rev.: Climate Change*, **8**, e474, https://doi.org/10.1002/wcc.474.

Gardner, M., 1970: Mathematical games. *Sci. Amer.*, **223**, 120–123, https://doi.org/10.1038/scientificamerican1070-120.

Haines, K., and J. C. Marshall, 1987: Eddy-forced coherent structures as a prototype of atmospheric blocking. *Quart. J. Roy. Meteor. Soc.*, **113**, 681–704, https://doi.org/10.1002/qj.49711347613.

Huang, C. S., and N. Nakamura, 2016: Local finite-amplitude wave activity as a diagnostic of anomalous weather events. *J. Atmos. Sci.*, **73**, 211–229, https://doi.org/10.1175/JAS-D-15-0194.1.

——, and ——, 2017: Local wave activity budgets of the wintertime Northern Hemisphere: Implication for the Pacific and Atlantic storm tracks. *Geophys. Res. Lett.*, **44**, 5673–5682, https://doi.org/10.1002/2017GL073760.

Jia, X., S. Yang, W. Song, and B. He, 2014: Prediction of wintertime Northern Hemisphere blocking by the NCEP Climate Forecast System. *J. Meteor. Res.*, **28**, 76–90, https://doi.org/10.1007/s13351-014-3085-8.

Kassam, A.-K., and L. N. Trefethen, 2005: Fourth-order time-stepping for stiff PDES. *SIAM J. Sci. Comput.*, **26**, 1214–1233, https://doi.org/10.1137/S1064827502410633.

Luo, D., 2000: Planetary-scale baroclinic envelope Rossby solitons in a two-layer model and their interaction with synoptic-scale eddies. *Dyn. Atmos. Oceans*, **32**, 27–74, https://doi.org/10.1016/S0377-0265(99)00018-4.

——, 2005: A barotropic envelope Rossby soliton model for block eddy interaction. Part I: Effect of topography. *J. Atmos. Sci.*, **62**, 5–21, https://doi.org/10.1175/1186.1.

Malguzzi, P., and P. Malanotte-Rizzoli, 1984: Nonlinear stationary Rossby waves on nonuniform zonal winds and atmospheric blocking. Part I: The analytical theory. *J. Atmos. Sci.*, **41**, 2620–2628, https://doi.org/10.1175/1520-0469(1984)041<2620:NSRWON>2.0.CO;2.

Masato, G., B. Hoskins, and T. Woollings, 2013: Winter and summer Northern Hemisphere blocking in CMIP5 models. *J. Climate*, **26**, 7044–7059, https://doi.org/10.1175/JCLI-D-12-00466.1.

McWilliams, J., 1980: An application of equivalent modons to atmospheric blocking. *Dyn. Atmos. Oceans*, **5**, 43–66, https://doi.org/10.1016/0377-0265(80)90010-X.

Methven, J., and P. Berrisford, 2015: The slowly evolving background state of the atmosphere. *Quart. J. Roy. Meteor. Soc.*, **141**, 2237–2258, https://doi.org/10.1002/qj.2518.

Mullen, S., 1987: Transient eddy forcing of blocking flows. *J. Atmos. Sci.*, **44**, 3–22, https://doi.org/10.1175/1520-0469(1987)044<0003:TEFOBF>2.0.CO;2.

Nakamura, H., and J. Wallace, 1993: Synoptic behavior of baroclinic eddies during the blocking onset. *Mon. Wea. Rev.*, **121**, 1892–1903, https://doi.org/10.1175/1520-0493(1993)121<1892:SBOBED>2.0.CO;2.

——, M. Nakamura, and J. Anderson, 1997: The role of high- and low-frequency dynamics in blocking formation. *Mon. Wea. Rev.*, **125**, 2074–2093, https://doi.org/10.1175/1520-0493(1997)125<2074:TROHAL>2.0.CO;2.

Nakamura, N., and A. Solomon, 2010: Finite-amplitude wave activity and mean flow adjustments in the atmospheric general circulation. Part I: Quasigeostrophic theory and analysis. *J. Atmos. Sci.*, **67**, 3967–3983, https://doi.org/10.1175/2010JAS3503.1.

——, and ——, 2011: Finite-amplitude wave activity and mean flow adjustments in the atmospheric general circulation. Part II: Analysis in the isentropic coordinate. *J. Atmos. Sci.*, **68**, 2783–2799, https://doi.org/10.1175/2011JAS3685.1.

——, and D. Zhu, 2010: Finite-amplitude wave activity and diffusive flux of potential vorticity in eddy mean flow interaction. *J. Atmos. Sci.*, **67**, 2701–2716, https://doi.org/10.1175/2010JAS3432.1.

——, and C. S. Huang, 2017: Local wave activity and the onset of blocking along a potential vorticity front. *J. Atmos. Sci.*, **74**, 2341–2362, https://doi.org/10.1175/JAS-D-17-0029.1.

——, and ——, 2018: Atmospheric blocking as a traffic jam in the jet stream. *Science*, **361**, 42–47, https://doi.org/10.1126/science.aat0721.

Pelly, J., and B. Hoskins, 2003: How well does the ECMWF ensemble prediction system predict blocking? *Quart. J. Roy. Meteor. Soc.*, **129**, 1683–1702, https://doi.org/10.1256/qj.01.173.

Petoukhov, V., S. Rahmstorf, S. Petri, and J. Schellnhuber, 2013: Quasiresonant amplification of planetary waves and recent Northern Hemisphere weather extremes. *Proc. Natl. Acad. Sci. USA*, **110**, 5336–5341, https://doi.org/10.1073/pnas.1222000110.

Pfahl, S., C. Schwierz, M. Croci-Maspoli, C. Grams, and H. Wernli, 2015: Importance of latent heat release in ascending air streams for atmospheric blocking. *Nat. Geosci.*, **8**, 610, https://doi.org/10.1038/ngeo2487.

Riboldi, J., C. Grams, M. Riemer, and H. Archambault, 2019: A phase locking perspective on Rossby wave amplification and atmospheric blocking downstream of recurving western North Pacific tropical cyclones. *Mon. Wea. Rev.*, **147**, 567–589, https://doi.org/10.1175/MWR-D-18-0271.1.

Scaife, A., and Coauthors, 2011: Improved Atlantic winter blocking in a climate model. *Geophys. Res. Lett.*, **38**, L23703, https://doi.org/10.1029/2011GL049573.

Shutts, G., 1983: The propagation of eddies in different jetstreams: Eddy vorticity forcing of 'blocking' flow fields. *Quart. J. Roy. Meteor. Soc.*, **109**, 737–761, https://doi.org/10.1002/qj.49710946204.

Swanson, K., 2000: Stationary wave accumulation and the generation of low-frequency variability on zonally varying flows. *J. Atmos. Sci.*, **57**, 2262–2280, https://doi.org/10.1175/1520-0469(2000)057<2262:SWAATG>2.0.CO;2.

Trenberth, K., 1986: An assessment of the impact of transient eddies on the zonal flow during a blocking episode using localized Eliassen–Palm flux diagnostics. *J. Atmos. Sci.*, **43**, 2070–2087, https://doi.org/10.1175/1520-0469(1986)043<2070:AAOTIO>2.0.CO;2.

Tung, K.-K., and R. Lindzen, 1979: A theory of stationary long waves. Part I: A simple theory of blocking. *Mon. Wea. Rev.*, **107**, 714–734, https://doi.org/10.1175/1520-0493(1979)107<0714:ATOSLW>2.0.CO;2.

Woollings, T., and Coauthors, 2018: Blocking and its response to climate change. *Curr. Climate Change Rep.*, **4**, 287–300, https://doi.org/10.1007/s40641-018-0108-z.

Yamazaki, A., and H. Itoh, 2009: Selective absorption mechanism for the maintenance of blocking. *Geophys. Res. Lett.*, **36**, L05803, https://doi.org/10.1029/2008GL036770.